Isotopes in Environmental and Health Studies
Vol. 42, No. 2, June 2006, 115–133

Taylor & Francis
Taylor & Francis Group

What are the instrumentation requirements for measuring the isotopic composition of net ecosystem exchange of CO_2 using eddy covariance methods?†

SCOTT R. SALESKA*†, JOANNE H. SHORTER‡, SCOTT HERNDON‡, RODRIGO JIMÉNEZ‡, J. BARRY McMANUS‡, J. WILLIAM MUNGER§, DAVID D. NELSON‡ and MARK S. ZAHNISER‡

†Department of Ecology and Evolutionary Biology and Institute for the Study of Planet Earth, University of Arizona, 1041 E Lowell Street, Tucson AZ 85721, USA
‡Aerodyne Research Inc., 45 Manning Road, Billerica, MA 01821, USA
§Department of Earth and Planetary Sciences and Division of Engineering and Applied Sciences, Harvard University, 20 Oxford Street, Cambridge, MA 02138, USA

(Received 28 February 2005; in final form 10 March 2006)

Better quantification of isotope ratios of atmosphere-ecosystem exchange of CO_2 could substantially improve our ability to probe underlying physiological and ecological mechanisms controlling ecosystem carbon exchange, but the ability to make long-term continuous measurements of isotope ratios of exchange fluxes has been limited by measurement difficulties. In particular, direct eddy covariance methods have not yet been used for measuring the isotopic composition of ecosystem fluxes. In this article, we explore the feasibility of such measurements by (a) proposing a general criterion for judging whether a sensor's performance is sufficient for making such measurements (the criterion is met when the contribution of sensor error to the flux measurement error is comparable to or less than the contribution of meteorological noise inherently associated with turbulence flux measurements); (b) using data-based numerical simulations to quantify the level of sensor precision and stability required to meet this criterion for making direct eddy covariance measurements of the $^{13}C/^{12}C$ ratio of CO_2 fluxes above a specific ecosystem (a mid-latitude temperate forest in central Massachusetts, USA); (c) testing whether the performance of a new sensor – a prototype pulsed quantum cascade laser (QCL) based isotope-ratio absorption spectrometer (and plausible improvements thereon) – is sufficient for meeting the criterion in this ecosystem. We found that the error contribution from a prototype sensor (~0.2 ‰, 1 SD of 10 s integrations) to total isoflux measurement error was comparable to (1.5 to 2×) the irreducible 'meteorological' noise inherently associated with turbulent flux measurements above this ecosystem (daytime measurement error SD of ~60 % of flux versus meteorological noise of 30–40 % for instantaneous half-hour fluxes). Our analysis also shows that plausible instrument improvements (increase of sensor precision to ~0.1 ‰, 1 SD of 10 s integrations, and increased sensor stability during the half-hour needed to integrate eddy covariance measurements) should decrease the contribution of sensor error to the point where it is less than the contribution from meteorological noise. This suggests that new sensors using QCL-based isotope ratio absorption spectroscopy should make continuous long-term observations of the isotopic composition of CO_2 fluxes *via* eddy covariance methods feasible.

Keywords: Calculation; Carbon-13; Carbon-dioxide; Fluxus; Measurement; Methods; Modelling

*Corresponding author. Tel.: +1-520-626-1500; Fax: +1-520-621-9190; Email: saleska@email.arizona.edu

†Extended version of the paper presented at the 1st International Workshop on 'Stable Isotope Ratio Infrared Spectrometry: New Developments and Applications' (SIRIS), 6–8 September (2004), Vienna, Austria.

Isotopes in Environmental and Health Studies
ISSN 1025-6016 print/ISSN 1477-2639 online © 2006 Taylor & Francis
http://www.tandf.co.uk/journals
DOI: 10.1080/10256010600672959

1. Introduction

Stable isotope ratios of carbon and oxygen in CO_2 have long been recognized as a tool for identifying sources and sinks of atmospheric CO_2 and for probing the processes and mechanisms that together control carbon cycling. In particular, the different isotopic composition of CO_2 in photosynthetic flux (F_{photo}) versus respiratory flux (F_{resp}) may be used to partition net ecosystem exchange flux (F_{NEE}) of CO_2 into these component fluxes, which in turn would allow analysis of the underlying mechanisms controlling these distinct processes [1]. Appropriate isotopic measurements would allow the simultaneous solution of the pair of equations:

$$F_{\text{NEE}} = F_{\text{photo}} + F_{\text{resp}} \tag{1a}$$

$$\delta_{\text{NEE}} \cdot F_{\text{NEE}} = \delta_{\text{photo}} \cdot F_{\text{photo}} + \delta_{\text{resp}} \cdot F_{\text{resp}} \tag{1b}$$

where F_x is an ecosystem flux component, and δ_x is the corresponding isotopic composition of F_x, (the subscript being NEE for net ecosystem exchange flux, photo for photosynthetic flux, and resp for respiratory flux).

This approach can be employed using measurements of isotopic composition of either the carbon or the oxygen in CO_2. Carbon-based partitioning is possible because the carbon isotopic composition of respiring organic matter often differs slightly from the organic matter being concurrently photosynthesized [2]. Oxygen-based partitioning is possible because the oxygen isotopic composition of soil water typically differs strongly from that of leaves [3–5]. Isotopic exchange between these leaf and soil waters and gas-phase CO_2 then means that the air surrounding photosynthesizing leaves will commonly have very different CO_2 isotopic composition ($\delta^{18}O_{CO2}$) than does the respired CO_2 from soils [6–8]. Choosing which tracer to use in such a partitioning involves trade-offs: the end-member pools determining carbon isotopic composition of net CO_2 flux may be directly characterized, but their differences are usually very small. The end-member water pools controlling the oxygen isotopic composition of net CO_2 flux are almost always very different (potentially leading to easily resolvable differences between flux components), but the relevant water pools are harder to define [9]. Prudent research strategy requires continuous measurements of isotopic composition of fluxes of both carbon and oxygen in CO_2. It may also be helpful for the CO_2 partitioning problem to measure the isotopic composition of the water flux, as this is related to the end member water pools which also influence $\delta^{18}O$ of CO_2 [10].

F_{net} is currently measured via eddy covariance methods continuously at hundreds of sites around the world, as part of the FLUXNET project (http://daac.ornl.gov/FLUXNET/), but measurements of the isoflux ($\delta_{\text{net}} \cdot F_{\text{net}}$) and the end-members δ_{photo} and δ_{resp} are more challenging and so far have been almost entirely limited to one-day experiments [1, 9, 11], multi-day but limited field campaigns [12], or long-term but sparse sampling [13–15]. Wider usage of stable isotopes in ecosystem exchange studies has been impeded by the labor intensive nature of standard methods using isotope ratio mass spectrometry (IRMS), which typically require samples to be collected in flasks and returned to the laboratory for analysis. Although recent advances in automated sample collection systems [2, 12, 14, 16, 17] make IRMS-based applications less cumbersome, direct *in situ* measurements made at high frequency are needed for eddy covariance applications. Tunable infrared laser differential absorption spectroscopy (TILDAS) describes a broad class of technologies which have been successfully applied to making eddy covariance flux measurements of trace gases such as CH_4, N_2O, and NO_2 [18–22] and which hold promise for the more difficult problem of measuring the isotopic composition of CO_2 fluxes as well.

Tunable diode laser absorption spectroscopy (TDLAS), a subset of TILDAS technologies, has recently been adapted for measurement of isotope ratios of atmospheric CO_2 and H_2O

vapour [10, 23–27]. These studies demonstrate the potential of technology that can make continuous in situ measurements. However, TDLAS instruments have not yet been employed in measuring eddy covariance fluxes because the need for frequent drift-correcting calibrations complicates the flux calculations that need to be integrated for as much as 30 min (at least in forest ecosystems). Concentration measurements are sufficient for obtaining gradients and, therefore, estimating fluxes over low-stature ecosystems with aerodynamically smooth vegetation cover such as grasslands and agricultural fields (e.g. Griffis *et al.* [26] calculated isotopic fluxes from gradients measured over a soybean field using lead-salt TDLAS technology), but for fluxes over tall vegetation ecosystems such as forests, this approach is logistically difficult because it would require concentration measurements well above the roughness sublayer, typically at an infeasibly high altitude for most tower-based measuring platforms. Hence, in forest ecosystems, the eddy covariance method is preferable. In addition, lead salt laser-based TDLAS technology is cumbersome and requires cryogenic cooling of the laser source. These characteristics make such technology less than ideal for taking full advantage of the principal strength of the eddy covariance method as a research tool, which is the ability to integrate continuous fluxes over extended time periods in remote field sites [28, 29].

A new generation of laser light sources, quantum cascade lasers (QCLs), can provide alternative sources of mid-infrared radiation that can overcome some of the difficulties associated with lead-salt diode lasers by providing near room temperature operation and increased power output. Since QCLs were first demonstrated [30], they have undergone rapid development [31] and can now provide the combination of high precision, long-term stability, and low temperature sensitivity that is needed for good-quality measurements at remote field sites [32, 33]. When operated in pulsed mode, QCLs overcome the limitations of lead-salt lasers by operating with single mode at near-room temperature and with highly stable mode output. Combining pulsed QCLs with thermoelectrically cooled infrared detectors results in a totally cryogen-free operation [32], a significant advantage for field deployment.

In this article, we define the instrumentation requirements for making direct eddy covariance measurements of isotopic composition of exchange fluxes and test the feasibility of making such measurements using absorption spectrometers built with the new generation of QCL light sources. Firstly, we review the technical requirements for making eddy covariance measurements of the isotopic composition of net ecosystem exchange between forest ecosystems and the atmosphere and propose a specific criterion for judging whether a sensor's performance is sufficient to achieve the kind of science goals typically pursued by such measurements.

Secondly, we describe the design of a prototype absorption spectrometer instrument that uses QCLs, and present data characterizing instrument performance in the laboratory in measuring $^{13}C/^{12}C$ isotope ratios in CO_2 at ambient concentrations. We also characterize the improved performance levels that we expect to achieve in a planned field-deployable isotope ratio instrument, based on current performance of a similar instrument already developed for ambient $^{12}CO_2$ concentration measurements from airborne platforms.

Finally, we use simulations to quantitatively define sensor performance requirements and test whether the performance of our isotope-ratio spectrometer (in both prototype and target development forms) meets the proposed criterion. We do this by (a) simulating the $^{13}C/^{12}C$-CO_2 isoflux above a real forest ecosystem (Harvard Forest, Central Massachusetts) from existing CO_2 eddy covariance measurements and from isotope data derived from flasks (giving a signal that for the purposes of sensor evaluation we treat as 'true'); (b) sampling from this simulation after adding 'measurement error' (where characteristics of the error term are derived from either theoretical statistical distributions or from laboratory tests of a specific sensor) and recalculating the isoflux (giving an estimate of the isoflux that would be 'measured'), and finally (c) comparing how closely the 'measured' isoflux approaches the 'true' (simulated) isoflux in light of the proposed criterion.

2. Methods

2.1 *Requirements for eddy covariance measurements*

Net ecosystem exchange (F_{NEE}) of CO_2 (in μmoles m^{-2} s^{-1}) is, under appropriate field conditions, typically estimated using eddy covariance methods as [34]

$$F_{\mathrm{NEE}} = \rho\overline{w'[\mathrm{CO_2}]'} + \rho\frac{\mathrm{d}}{\mathrm{d}t}\int_0^h [\mathrm{CO_2}](z)\mathrm{d}z \tag{2}$$

where ρ is molar density of air (moles m^{-3}), $\overline{w'[\mathrm{CO_2}]'}$ (in ppm m s^{-1}) is the w-CO_2 covariance (w being vertical wind in m s^{-1} and $[CO_2]$ being the molar concentration of carbon dioxide, both taken at a height h, a position above the top of the canopy) during an averaging period (typically 30 min), and the second term on the right is the storage flux, the change in the CO_2 column stored in the canopy air below height h. The primes in the covariance term derive from Reynolds decomposition, by which a timeseries $x(t)$ is rewritten (over some time period) as $\overline{x} + x'(t)$, where the $x'(t)$ are fluctuations from the mean value across the time period (and, in practice, the explicit time index is often omitted, as in equation (2). CO_2 is transported when CO_2 fluctuations in one direction are consistently associated with fluctuations in vertical wind, (e.g. during night time efflux, vertical wind, and CO_2 are positively correlated). The storage flux can be especially important in tall vegetation, such as forests, when attempting to measure the hour-by-hour flux without bias. However, as the purpose of this article is to assess sensor requirements for measuring eddy covariances (not to estimate net ecosystem exchange), we neglect the consideration of a storage flux term in what follows.

The isotopic analog to equation (2), expressed in common isotopic notation (in units of μ moles CO_2 m^{-2} s^{-1} ‰) is [13, 35]

$$\delta_{\mathrm{NEE}} F_{\mathrm{NEE}} = \rho\overline{w'(\delta^{13}\mathrm{C}\cdot[\mathrm{CO_2}])'} + \rho\frac{\mathrm{d}}{\mathrm{d}t}\int_0^h \left(\delta^{13}\mathrm{C}(z)\cdot[\mathrm{CO_2}](z)\right)\mathrm{d}z \tag{3}$$

where $\delta^{13}C$ is the $^{13}C/^{12}C$ ratio of $[CO_2]$, conventionally expressed as a deviation, in parts per thousand (‰), from a standard ratio ($\delta^{13}\mathrm{C} = [^{13}\mathrm{C}/^{12}\mathrm{C} - R_{\mathrm{PDB}}]/R_{\mathrm{PDB}}$, where R_{PDB} is the international standard), and the other symbols are as previously defined. The terms in equation (3), derived from the mass balance of $^{13}CO_2$, are often called isofluxes, and a complete measurement of net ecosystem isoflux (left-hand side term) requires measurements of both eddy isoflux and storage isoflux. In the remainder of the article, we focus on assessing sensor performance in measuring eddy isofluxes (the first term on the right-hand side). For simplicity in what follows, we neglect the effect of molar air density ρ and report raw covariances (p.p.m. m s^{-1} for CO_2 eddy flux and p.p.m. m s^{-1} ‰ for eddy isoflux).

Eddy covariance measurements impose strong technical requirements on sensor technology, including (1) rapid response time (<1 s, sufficient to capture the high-frequency transport flux); (2) sensor stability (sufficient to integrate continuous measurements without drift over a sufficiently long time to capture the low-frequency transport flux); and (3) high precision (so that the small fluctuations that constitute the eddy flux signal can be resolved).

Spectral analysis of eddy covariance flux data for CO_2 and H_2O at Harvard Forest shows that 2 Hz sampling is adequate to capture most high-frequency fluctuations and that 30 min integration periods are adequate to capture most low-frequency fluctuations [34]. As laser absorption spectroscopy systems routinely acquire data at 10 Hz or more, sensor response time is not a technical hurdle for making spectroscopically-based isotope ratio measurements. Low stability of traditional lead-salt laser technology, however, means that frequent calibrations (every several minutes) are required [24, 26], making it difficult to achieve 30 min of

uninterrupted integration time to capture the low-frequency fluctuations. The inherent stability of QCLs relative to lead-salt technology offers the potential for an absorption spectrometer that can integrate isotope ratio measurements over the necessary time period without excess drift.

The need for precise high-resolution measurements (requirement 3) poses a technical challenge for eddy covariance measurements of isotope ratios because it is crucial that the differences in atmospheric concentration between updrafts and downdrafts be adequately resolved.

In order to judge whether the sensor's performance is adequate to meet these requirements, we propose an objective 'sensor performance' criterion. This sensor-performance criterion asks: is the portion of variation in measured eddy isoflux that is attributable to sensor error (which may arise from either sensor drift or lack of resolution) comparable to or less than the portion of the variation attributable to meteorological noise inherently associated with turbulence flux measurements? If the answer is yes, the criterion is satisfied; the sensor is as good as it needs to be to achieve flux measurements of maximum resolution in a given ecosystem, as further reductions in sensor error cannot give improvements in total isoflux error because such improvements are limited by the irreducible noise of turbulent fluxes.

2.2 *QCL spectrometer*

2.2.1 Prototype instrument and performance. The design principles and construction details for our prototype QCL spectrometer are discussed in McManus *et al.* [36], but we briefly review them here. The instrument (figure 1) combines a commercially available QCL (ALPES Lasers, www.alpeslasers.com) operated in pulse mode, an optical system, and a computer-controlled system that incorporates the electronics for driving the QCL along with signal generation and data acquisition. The spectrometer is devised for simultaneous measurement of absorption (sample), pulse normalization (reference), and frequency-lock spectra from the QCL. The laser used here can be tuned to the infrared frequencies between 2310 and 2315 cm^{-1}. On the basis of a suite of selection criteria discussed in McManus *et al.* [36, 37], we used a pair of CO_2 absorption lines near 2311 cm^{-1} (2311.399 cm^{-1} for $^{13}CO_2$ and 2311.105 cm^{-1} for $^{12}CO_2$), as suggested by Weidmann *et al.* [38].

A key feature of the design of the optical system is a dual-path multi-pass cell which compensates for the large (factor of 100) difference in concentration between major and minor isotopologues of CO_2. Our approach, previously implemented with a conventional lead-salt diode laser [37], uses path lengths that differ by a factor of 74, implemented with a multi-pass astigmatic Herriott cell (base length 0.32 m) in which the different path lengths (0.753 and 56.08 m) are defined by the number of cell passes (either 2 or 174). This approach overcomes a significant problem in the spectroscopic measurement of isotopic abundances, as the measurement of two isotopic species using lines of similar strength but very unequal concentrations leads to low accuracy, with either the minor constituent having too small an absorption depth or the major constituent having too great an absorption depth. If lines with unequal strength are chosen to compensate for the absorption depth imbalance, then accuracy tends to suffer because of the greater temperature sensitivity of the weaker strength line. Here, the dual path approach greatly lessens the effect of temperature variations in the instrument environment; the temperature stability requirement is virtually negligible (180 K/0.1 ‰) using the chosen line pairs at 2311 cm^{-1}.

Absolute spectroscopic mixing ratios are calculated using the HITRAN data base parameters [40], the measured pressure, temperature, path lengths, and the laser line width. The laser line width is convolved with the molecular absorbance model during the fitting to account for non-linear effects at higher optical depths. The isotopologue line strengths in HITRAN are scaled

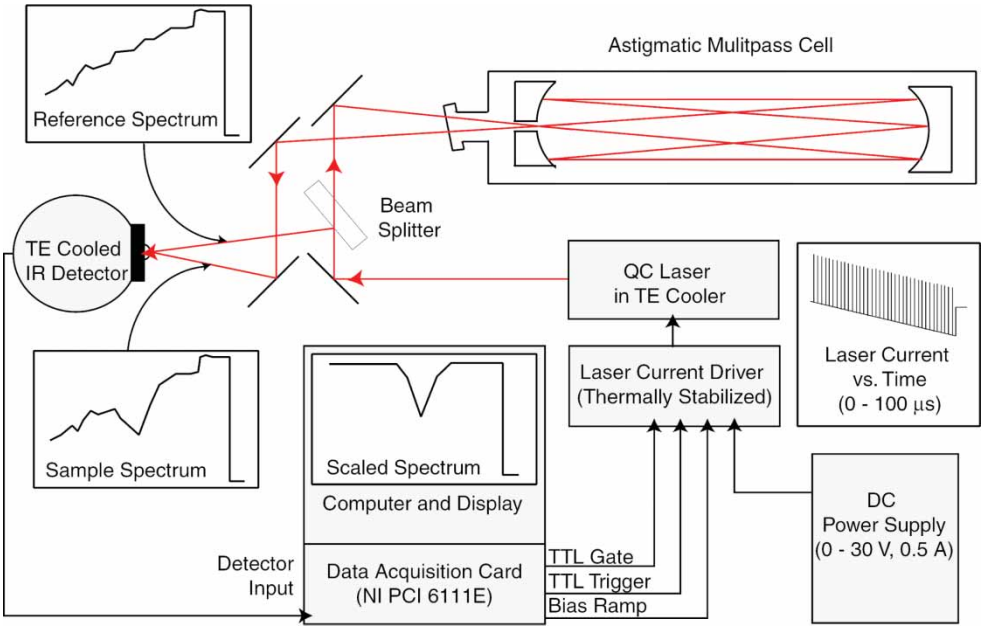

Figure 1. Schematic for prototype isotope-ratio QCL absorption spectrometer [36].

by their nominal natural abundances. For $^{13}CO_2$ this scaling factor is $R_{PDB} = 0.01124$, the ratio of the Pee Dee Belemnite (PDB) international standard. Directly retrieved mixing ratios are typically within $\sim$5 % of true values even with no rescaling or calibration (e.g. directly retrieved mixing ratios for 350 p.p.m. reference air were 345 p.p.m. for $^{12}CO_2$ and 333 p.p.m. for $^{13}CO_2/0.01124$). However, high-accuracy applications like those proposed here would require routine calibration for both isotopologues to account for residual uncertainties in the laser line shape and absorption baseline.

We evaluated the long-term stability of the prototype QCL using the Allan variance technique [41, 42], which distinguishes high-frequency random variations in the measurement from systematic variations at longer time scales. To summarize briefly, on a log–log plot in which the variance of repeated measurements of a sample with fixed concentration or isotope ratio is plotted against the averaging time t over which each of those repeated measurements is averaged (called an Allan plot, see lower panel of figures 2 and 3), the variance will generally decrease with time if the measurement error is random because integrating over longer times will average away random fluctuations. If measurement error is a pure random white noise (with a power spectrum that is a constant independent of frequency), the variance (σ^2) will decrease with t^{-1} (σ decreases as $t^{-1/2}$), and a log–log plot of variance versus integration time would be expected to have a slope of -1. If measurement errors are random but correlated, then the measurement variance will still decrease, but not as rapidly (in particular, in the case of so called 'pink noise,' which has a power spectrum $\sim 1/f^{0.5}$, where f is frequency, the variance falls with a slope of $-1/2$). If there are systematic drifts at longer timescales due to temperature, optical instability, or laser instability, then repeated measurements averaged at those time-scales or longer will be systematically different from each other (because of the drift) and hence have larger and larger variances. The integration time (called τ_{Allan}) at which the minimum variance occurs (called σ^2_{Allan}) characterizes instrument stability and defines a time-scale that divides the time domain into a region in which random noise fluctuations can be averaged over ($t < \tau_{Allan}$) and a region ($t > \tau_{Allan}$) in which systematic drift dominates. Measurement errors

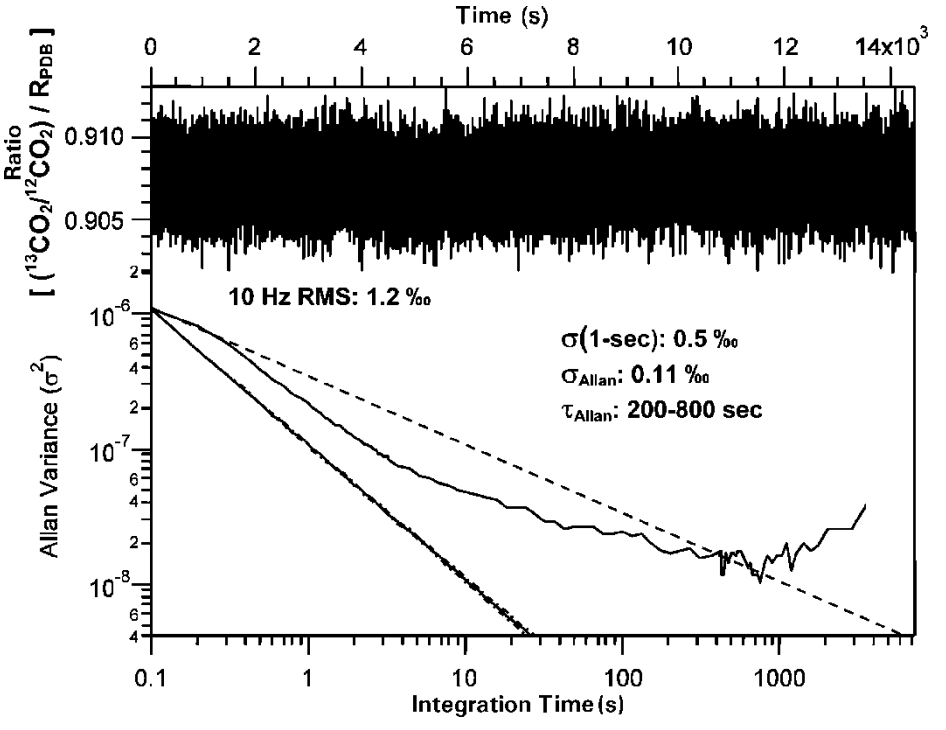

Figure 2. 10 Hz isotope ratio time series (upper plot) and corresponding Allan variance plot (lower) of a 4 h time series collected by prototype $^{13}CO_2/^{12}CO_2$ QCL sensor with ambient air sealed in the sample cell at 7 torr. Downward sloping straight lines on the Allan plot show the theoretical behavior for white noise (slope-1) and pink noise (slope-1/2) processes.

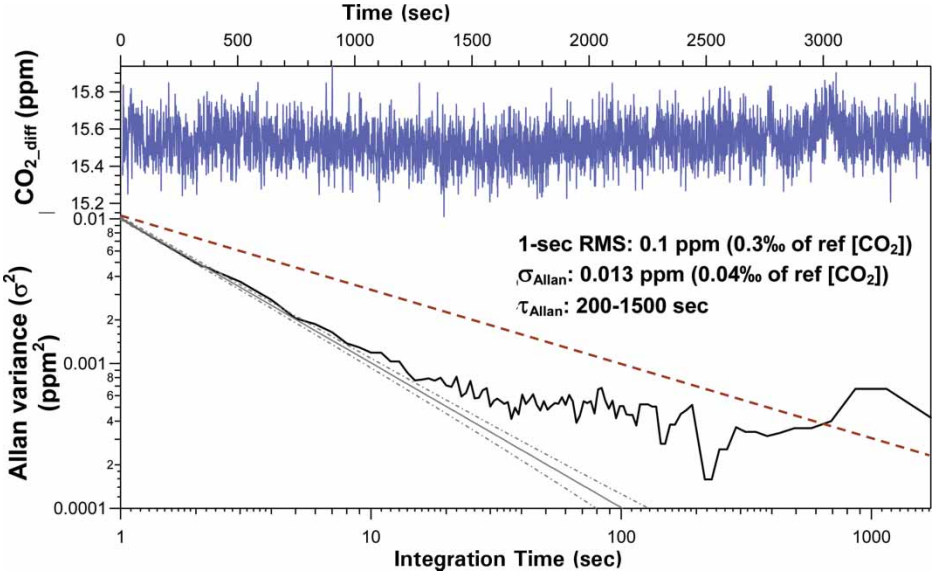

Figure 3. Time series (upper plot) of CO_{2-diff} (the difference between sample and reference air, taken from two different tanks, sampled at 1 Hz) and corresponding Allan variance plot (lower) for $^{12}CO_2$ measured by a CO_2 QCL sensor [43]. 1 s RMS noise and Allan variance minima are expressed in p.p.m. and, in parentheses, as a fraction (in parts per thousand, ‰) of the reference gas concentration (ref. $[CO_2] = 375$ p.p.m.). Downward sloping straight lines on the Allan plot show the theoretical behavior for white noise (slope-1, bracketed by dot–dash lines showing the 95% confidence interval) and pink noise (slope-1/2) processes.

due to systematic drifts should be corrected by periodic external calibrations using reference gas with known concentration and isotope ratio, with τ_{Allan} useful in choosing an optimal calibration frequency for maintaining long-term precision.

A 10 Hz time series and Allan plot of the $^{13}CO_2/^{12}CO_2$ ratio are shown in figure 2 for a 4 h period with ambient air sealed in the sampling cell at 7 Torr. The time series of the $^{13}CO_2/^{12}CO_2$ ratio has a 0.1 s RMS of 1 ‰ which ideally would decrease to 0.1 ‰ after 10 s if measurement error was random white noise. However, the measurement error behaves like a process intermediate between white noise and $1/f^{0.5}$ 'pink' noise, indicating that that there are some correlations in noise sources at time scales of 0.1–100 s (figure 2). The variance has a broad minimum between at 200 and 800 s with a minimum corresponding to $\sigma_{\text{Allan}} = 0.11$ ‰. There is a greater proportional decrease from 1 to 200 s for the isotope ratio than for either of the isotopologues measured separately (not shown), indicating that some of the contributing noise sources such as laser line width variation and peak position stability are correlated and cancel when the ratio is taken.

2.2.2 Development target instrument and performance. Figure 2 characterizes the performance of our prototype isotope ratio QCL spectrometer. We believe that further modifications to instrument design can improve on this performance, and we describe here the characteristics of a 'development target' instrument incorporating these improvements. In particular, we note that the existing prototype design has no reference cell. The addition of reference cells (one paired with each path in the sample cell) with column densities roughly equal to that in the corresponding sample path should increase measurement stability and precision. This is because the largest sources of noise in the 1–100 s time scales are residual laser frequency fluctuations affecting both the peak position and the laser line width. As the magnitude of these uncertainties will scale directly with the absorption area, reducing the absorption area by dividing the sample cell spectrum by a reference spectrum obtained from an equal column density reference cell will increase measurement precision.

This technique of reference cell normalization has been employed before in absorption instrumentation (e.g. the widely used Licor CO_2 infrared gas analyzer, though not a spectroscopic instrument, achieves high precision with matched sample and reference cells, and the same principle is used in a commercially-available isotope-ratio spectrometer using conventional lead-salt technology [24, 26]. We are implementing this technique with QCL technology in a high-precision $^{12}CO_2$ QCL sensor currently under development for deployment on aircraft [43]. This sensor measures only the $^{12}CO_2$ isotopologue, but the technology is otherwise similar to the prototype isotope ratio instrument discussed above.

The $^{12}CO_2$ aircraft sensor operates in difference mode using two matched 10 cm cells (one for sample air and one for a known reference) and dividing sample spectrum by reference spectrum before fitting. We plan to apply the same technique to the isotope ratio spectrometer, by adding two 10 cm path cells – one flushed with 0.2 % CO_2 reference gas (to balance the short path), and one flushed with 20 % CO_2 reference gas (to balance the long path), in future work. Balancing the absorption before spectral fitting will minimize sensitivity to laser linewidth changes and frequency stability in the lasers. For the purposes of this article, we quantify the effects of planned improvements in order to simulate their effects on measured eddy covariance fluxes.

We quantify the improvement expected from this potential modification by considering the performance of the existing $^{12}CO_2$ QCL sensor [43]. As discussed above, this sensor is designed to measure absolute $^{12}CO_2$ concentrations only, not isotope ratios, but the technique of reference cell normalization should have comparable stabilizing effects on $^{13}CO_2$ isotopologue. Thus, the characteristics of the existing $^{12}CO_2$ QCL instrument allow us to conservatively define the expected performance of a 'development target' isotope ratio spectrometer.

The Allan plot for this sensor (figure 3) shows a lower 1 s RMS noise (0.1 p.p.m. CO_2 or about 0.3 ‰ of ambient), a more rapid initial decrease (along the t^{-1} line between 1 and 30 s), and a greater long-term stability (the minimum approached at 200 s remains virtually flat to ∼1500 s) than in the prototype isotope ratio spectrometer (figure 2). The minimum corresponds to a precision of 0.014 p.p.m. or 0.04 ‰ of ambient CO_2. Such an instrument should allow us to obtain an RMS precision on isotope ratios of 0.1 ‰ with 10 s averaging time and to push calibration intervals to 1500 s (25 min). Calibrations would be interspersed between each separate eddy covariance integration to ensure long-term stability in isotopic measurements.

A summary of relevant specifications and performance characteristics in the prototype and development target spectrometers (compared to a closely related commercially available alternative) is in table 1.

2.3 *Simulation methods*

2.3.1 Simulating isoflux and associated measurement error. Firstly, we simulate the $^{13}C/^{12}C$-CO_2 isoflux above a real forest ecosystem (Harvard Forest, Central Massachusetts)

Table 1. Instrument characteristics of demonstrated lab prototype, conservatively estimated development target, and the most closely related commercially available alternative.

	Lab prototype†	Development target‡	Reference Current commercial state-of-the-art§
Laser light source			
Laser type	Pulsed QC infrared laser		Continuous-wave lead-salt diode
Tuning range	2310–2315 cm^{-1}		
Absorption lines	$^{13}CO_2$: 2314 or 2311 cm^{-1}		2308 cm^{-1}
Temperature stability required for above line	(0.2 K) or (180 K) per 0.1 ‰		(0.006 K) per 0.1 ‰
Scan rate	4 kHz		0.5 kHz
Simultaneous dual laser mode operation	***No***	***Yes***	No
Optical cell			
Laser path length	Dual paths: 0.74 and 56 m		1.5 m
Matched reference cell	***None***	***Dual***	Yes
Measurement performance			
1 s 1σ precision (‰)	0.5	0.4	0.4
10 s 1σ precision (‰)	0.2	0.1	0.1
Allan variance minimum (σ_{Allan}) (‰)	0.1	0.05	0.1
Stability, as given by time to Allan σ minimum (τ_{Allan}) (s)	∼200–800	200–1500 (flat)	30
	(provides an indicator of time interval between calibrations)		
Response time (s)	0.1 or faster		0.1
Physical specifications and design features			
Cooling of laser	Thermoelectric (TE)	TE	LN_2
Cooling of detector	***LN_2***	***TE***	TE
Weight (incl. electronics) (kg)	75		75
Analyzer unit dimensions (m^2)	0.65 × 0.40		2.1 × 0.55

Note: Key development modifications to improve performance of the prototype are indicated in ***bold italics*** and key advantages for field deployment and eddy-covariance measurements, relative to the current state-of-the-art, are shaded in gray.

†Prototype performance assessed from data in figure 2.
‡Development target characteristics are conservatively estimated on the basis of demonstrated performance (figure 3) of a similarly designed Aerodyne QC-TILDAS sensor for aircraft-based CO_2 concentration measurements [43].
§TGA-100, Campbell Scientific (Logan, Utah) [24].

from existing CO_2 eddy covariance measurements and from isotope data derived from flasks. Net ecosystem exchange of CO_2 (NEE) has been measured by eddy covariance at Harvard Forest since 1991, and the site, measurement methods, and analysis are described in detail in other publications [28, 34]. Periodic measurements of the concentration and isotopic composition of atmospheric CO_2 at Harvard Forest are reported in Lai *et al.* [15] and exhibit a well-defined relation, in which $\delta^{13}C$ is proportional to $1/[CO_2]$ (figure 4(A)), known as a Keeling plot relation. From the long-term eddy flux data set and the $\delta^{13}C$ versus CO_2 relation, we simulate the high-frequency carbon isotope ratio time series ($\delta^{13}C_{sim\_true}$) and from this calculate the half-hourly isoflux, $\overline{w'(\delta^{13}C_{sim\_true} \cdot [CO_2])'}$, following a method essentially the same as that used by Ogee *et al.* [9], and similar to an approach first used by Bowling *et al.* [2], who used a regression linear in $[CO_2]$ rather than in $1/[CO_2]$. For the purposes of sensor evaluation we treat this simulated isoflux as 'true'.

Next, in order to quantify the effect of sensor error, we simulate the measured isoflux by adding measurement error to the simulated 'true' $\delta^{13}C_{sim\_true}$ time series:

$$\delta^{13}C_{sim\_meas}(t) = \delta^{13}C_{sim\_true}(t) + \varepsilon(t) \tag{4}$$

and then recalculating the isoflux as $\overline{w'(\delta^{13}C_{sim\_meas} \cdot [CO_2])'}$. We use four different error time series for $\varepsilon(t)$: $\varepsilon_{prot}(t)$, the actual prototype instrument error (the ratio time series in the

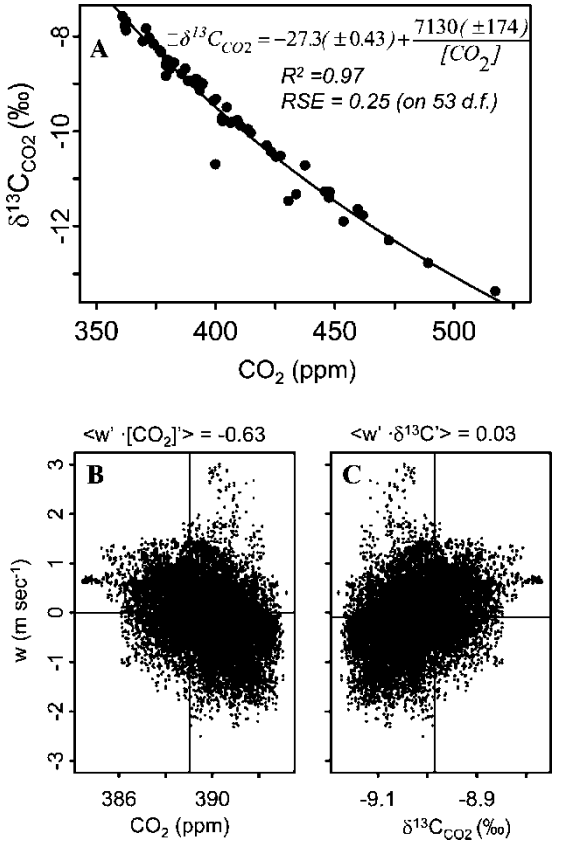

Figure 4. (A) Summer 2003 Harvard forest $\delta^{13}C$ versus $[CO_2]$ (above canopy air sampled by flasks [15]) gives a relation allowing simulation of high-frequency $\delta^{13}C$ from CO_2. (B) Actual w-CO_2 covariance and (C) Simulated w-$\delta^{13}C$ covariance (where $\delta^{13}C$ is derived from the regression in (A)) illustrating the relatively small range of expected $\delta^{13}C$ variation in a typical daytime half-hour (~0.4‰). Data in (B) and (C) is from 2 July 2003, 1300–1330 h.

upper plot of figure 2); $\varepsilon_{\text{develop}}(t)$, the error associated with the 'development target' instrument (derived from the time series in figure 3); $\varepsilon_{\text{pink}}(t)$, a random 'pink noise' time series generated by inverse-Fourier transforming a white noise power spectrum scaled by density $1/f^{0.5}$ into the time domain; $\varepsilon_{\text{white}}(t)$, a random white noise process. The simulated noise series', $\varepsilon_{\text{pink}}(t)$ and $\varepsilon_{\text{white}}(t)$, allow us to quantify the contribution of sensor error to total isoflux error over a range of magnitudes for sensor error and to identify the largest sensor error that would still satisfy the 'sensor-performance' criterion discussed at the end of section 2.1. The instrument error series', $\varepsilon_{\text{prot}}(t)$ and $\varepsilon_{\text{develop}}(t)$, allow us to test the performance of actual instruments relative to this criterion. One caveat is that $\varepsilon_{\text{prot}}(t)$ and $\varepsilon_{\text{develop}}(t)$ are based on the measurements on gas sealed in the instrument for several hours in the lab, whereas field measurements will be on sample air flowing rapidly through the sample cell. Effects such as temperature fluctuations in the flowing sample air could cause larger measurement error, but as closed-path field instruments for eddy flux measurements are typically designed to stabilize sample gas temperature, we anticipate that such an effect in a properly designed instrument should be very small.

The 'development target' error series $\varepsilon_{\text{develop}}(t)$ was generated from the $CO_{2\_\text{diff}}(t)$ time series in figure 3 as follows:

$$\varepsilon_{\text{develop}}(t) = \sqrt{2} \cdot \frac{[CO_{2\_\text{diff}}(t) - CO_{2\_\text{diff}}(t)]}{CO_2(\text{reference})} \tag{5}$$

where $[CO_2(\text{reference})]$ is the CO_2 concentration in the reference tank (close to ambient, ~375 p.p.m.) and $CO_{2\_\text{diff}}(t)$ is the measured difference between sample air and $[CO_2(\text{reference})]$. $\varepsilon_{\text{develop}}(t)$ is expressed as per mil deviation from the mean, relative to the concentration being measured; it is inflated by $\sqrt{2}$ to account for effect of taking a ratio with a hypothetical independent $^{13}CO_2$ series with similar noise characteristics; $\varepsilon_{\text{develop}}(t)$ has mean zero and standard deviation 0.42‰ (=1 s RMS noise). We believe this error series to be a conservative estimate of the likely performance of a dual reference cell $^{13}CO_2/^{12}CO_2$ QCL spectrometer because it assumes that errors on the two isotopologues series are independent (hence the $\sqrt{2}$ inflation of the actually measured series in figure 3). In contrast, the ratio time series from the prototype sensor exhibits improved noise characteristics relative to the individual time series, apparently due to canceling of correlated errors, but this effect may be smaller in a development target sensor because each individual series will already be the ratio of sample and reference cells.

The magnitude of simulated isoflux measurement error was quantified using the 'bootstrap' technique [44], i.e. by repeating the isoflux recalculation for each of 100 bootstrap resamples on each half-hour and taking the standard deviation of the 100 bootstrapped isofluxes, where each resample was generated with an independent realization of the appropriate error time series.

2.3.2 Separating total Isoflux variability into sensor error versus sample variation. To assess whether the sensor-performance criterion was met, we compared the magnitude of half-hourly sensor-induced measurement error to the magnitude of 'meteorological' noise. We quantified meteorological noise as the standard deviation of the simulated 'true' isoflux (i.e. without measurement noise added) across different half-hours with similar environmental driving variables (photosynthetically active radiation, PAR), where 'representative' half-hours were taken from within a given day (within 1 h on either side) and from nearby measurement days (within 5 days on either side).

In addition to simulating half-hourly isoflux measurements on a given day, we also calculated 10-day hourly diurnal patterns of isoflux, a common approach to characterizing ecosystem properties using noisy eddy covariance data [45] that facilitates analysis of how mean flux

patterns respond to changes in mean diurnal patterns of driving variables such as moisture, temperature, and sunlight. We analyzed the overall variability in simulated measured hourly means across the 10-day averaging period by dividing the total variability into two components: sample variation (the variation in 'true' isoflux for a given hour across the 10 measurement days due to day-to-day variations in environmental conditions and turbulent noise) and sensor error (the uncertainty on flux for a given single hour, quantified as the variation across 100 bootstrap 'remeasurements' of that hour generated according to the method of the previous section).

Total variance on each hour of the day, σ^2_{Tot}, can be partitioned as follows: let F_{dj} be the isoflux for a given hour (e.g. 10 a.m.) on the dth day (where d ranges from 1 to n_{day}) and the jth bootstrap simulation on that day (where j ranges from 1 to n_{boot}). Then the grand mean flux for that hour, across all days and bootstrap resamples, is

$$\overline{F} = \frac{1}{N_{\text{Tot}}} \sum_{d=1}^{n_{\text{day}}} \sum_{j=1}^{n_{\text{boot}}} F_{dj}$$

where $N_{\text{Tot}} = n_{\text{boot}} \cdot n_{\text{day}}$, and the inner sum is just the mean flux on day d,

$$\overline{F_d} = \frac{1}{n_{\text{boot}}} \sum_{j}^{n_{\text{boot}}} F_{dj}.$$

The total variance of the grand mean flux

$$\sigma^2_{\text{Tot}} = \frac{1}{(N_{\text{Tot}} - 1)} \sum_{d}^{n_{\text{day}}} \sum_{j}^{n_{\text{boot}}} (F_{dj} - \overline{F})^2$$

can then be partitioned into the variance due to bootstrap variation ($\overline{\sigma^2_{\text{sensor}}}$ which here represents variation due to sensor measurement error) and the variance from day-to-day variations (σ^2_{day}) by following standard statistical methods for partitioning the sum-of-squared errors into their component errors

$$\begin{aligned}
\sigma^2_{\text{Tot}} \approx \frac{1}{N_{\text{Tot}}} \sum_{d}^{n_{\text{day}}} \sum_{j} (F_{d,j} - \overline{F})^2 &= \frac{1}{N_{\text{Tot}}} \left\{ \sum_{d}^{n_{\text{day}}} \sum_{j}^{n_{\text{boot}}} [(F_{dj} - \overline{F_d}) + (\overline{F_d} - \overline{F})]^2 \right\} \\
&= \frac{1}{N_{\text{Tot}}} \left\{ \sum_{d}^{n_{\text{day}}} \sum_{j}^{n_{\text{boot}}} [(F_{dj} - \overline{F_d})^2 + (\overline{F_d} - \overline{F})^2] \right\} \\
&= \frac{1}{n_{\text{day}} n_{\text{boot}}} \left[\sum_{d}^{n_{\text{day}}} \sum_{j}^{n_{\text{boot}}} (F_{d,j} - \overline{F_d})^2 + \sum_{d}^{n_{\text{day}}} n_{\text{boot}} (\overline{F_d} - \overline{F})^2 \right] \\
&= \frac{1}{n_{\text{day}}} \sum_{d}^{n_{\text{day}}} \sigma^2_{\text{sensor}(d)} + \frac{1}{n_{\text{day}}} \sum_{d}^{n_{\text{day}}} (\overline{F_d} - \overline{F})^2 \\
&= \overline{\sigma^2_{\text{sensor}}} + \sigma^2_{\text{day}} \qquad (6)
\end{aligned}$$

where we have used the definitions

$$\sigma^2_{\text{day}} = \frac{1}{n_{\text{day}}} \sum_{d}^{n_{\text{day}}} (\overline{F_d} - \overline{F})^2 \text{ (sample variance across days) and}$$

$$\sigma^2_{\text{sensor}(d)} = \frac{1}{n_{\text{boot}}} \sum_{j}^{n_{\text{boot}}} (F_{dj} - \overline{F_d})^2$$

(sensor measurement variance on day d). Note that in moving from lines 1 to 2 of equation (6), the cross term $2(F_{dj} - \overline{F_d})(\overline{F_d} - \overline{F})$ resulting from squaring the expression in line 1 is eliminated when the sums are taken.

The standard error for each hour across the n_{day} days is then $\text{SE}_{\text{Tot}} (= \sigma_{\text{Tot}}/\sqrt{n_{\text{day}}})$ and the sample and sensor measurement standard errors are $\text{SE}_{\text{sample}} (= \sigma_{\text{day}}/\sqrt{n_{\text{day}}})$, and $\text{SE}_{\text{sensor}} (= \overline{\sigma_{\text{sensor}}}/\sqrt{n_{\text{day}}})$.

3. Results and discussion

The measured eddy covariance CO_2 flux and the corresponding simulated half-hourly eddy isoflux (figure 5) show that (1) the error structure associated with the existing prototype instrument (figure 2) can generate a time series of half-hour flux measurements (figure 5) that is unbiased (figure 6(A)) and which has an isoflux uncertainty per daytime half-hour that is ~2 times the irreducible 'meteorological' noise inherently associated with turbulent fluxes (figure 6(B)); and (2) the 'development target' for the isotope ratio QCL sensor (based on performance already demonstrated with the $^{12}CO_2$ QCL sensor, figure 3) would enable isoflux measurements that approach the best precision that can be achieved given the inherent uncertainty introduced by atmospheric turbulence (figure 6(B)). Prototype coefficient of variation (CV, the ratio of standard deviation to the mean value) falls close to that produced by a pink noise with the same 1 s RMS, while development target characteristics fall in between white and pink noise.

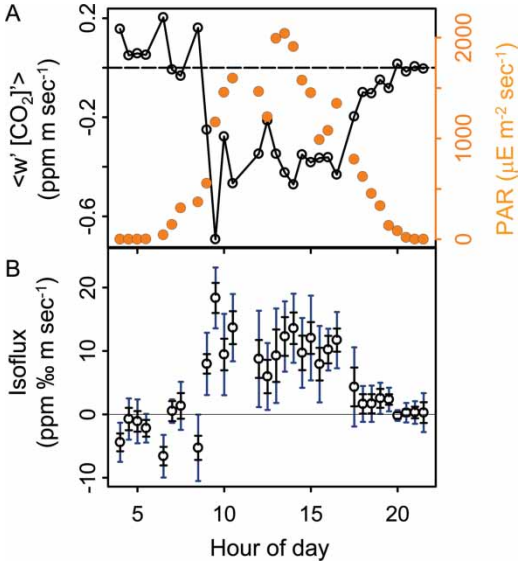

Figure 5. (A) Half-hourly measured covariance between vertical wind and CO_2 (open circles connected by lines, left scale), along with photosynthetically active radiation (PAR) (solid circles, right scale) on 15 July 2003. (B) Half-hourly simulated isoflux covariance, $\overline{w'(\delta^{13}C[CO_2])'}$, on the same day, including ±1 SD uncertainty due to measurement error in (i) prototype sensor (larger error bars) and (ii) 'development target' sensor (smaller error bars).

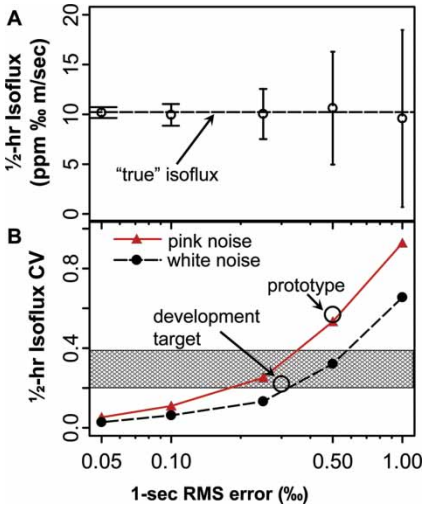

Figure 6. (A) Simulated half-hourly isoflux (for 1330–1400, 2 July 2003), including ±1 SD uncertainty (simulated from pink noise error series with spectral density $\sim 1/f^{0.5}$) versus 1 s RMS error and (B) corresponding half-hourly isoflux coefficient of variation (CV = SD/mean) as a function of 1 s RMS error for both white noise (circles) and pink noise (triangles) processes and for prototype and development target sensor characteristics. The hatched shaded horizontal bar is the range of uncertainty induced by meteorological fluctuations and is the irreducible noise inherently associated with turbulent flux measurements.

In evaluating the suitability of a sensor for eddy covariance measurements, it is useful to recognize that the ability of a sensor to resolve fluctuations in the scalar being measured should be evaluated based, not on the sensor's high-frequency (e.g. 0.1 s) RMS error, but on the integrated (e.g. 30 min) RMS error over the full averaging period. In other words, it is not necessary that high-frequency fluctuations be resolvable at high frequency, only that their covariance with wind be resolvable on average. This fact, long understood [46], is still sometimes underappreciated. In our case, in the terminology of equation (6), it is the quantity σ_{sensor} (the standard error on the mean 'true' covariance $\overline{w'(C\delta)'}$, where C is the CO_2 concentration and δ its isotopic composition) that must be sufficiently small. If the quantities w and (Cδ) are measured with sensor errors $\varepsilon(w)$ and ε(Cδ), then in the absence of spectral distortion or correlated errors between the two sensors (which must be absent for the eddy flux measurement method to work at all), the error on the covariance can be propagated from the 'bottom-up' and approximated (neglecting second-order terms) as $\sigma^2_{\text{sensor}} \approx S^2_{w'} S^2_{\overline{\varepsilon(C\delta)'}} + S^2_{(C\delta)'} S^2_{\overline{\varepsilon(w')}}$, where terms like $S_{x'}$ are the standard deviation of the high-frequency fluctuations in quantity x and terms like $S_{\overline{\varepsilon(x')}}$ (with an overbar on the subscript) are the standard error of $\varepsilon(x')$ for the sensor measuring x, after averaging over the full integration period. The $S_{x'}$ terms are site-dependent and thus not affected by sensor characteristics. $S_{\overline{\varepsilon(x')}}$ for an arbitrary integration period is by definition the square root of the Allan variance (e.g. figures 2 and 3) for that integration period and can be substantially lower than the standard error associated with high-frequency measurements.

The simulation demonstrates this concept numerically: development target performance includes a 1 s RMS noise of 0.4 ‰, approximately equal to the whole range of the simulated isotope fluctuations in figure 4(C); clearly no individual high-frequency points could be resolved with this comparatively low high-frequency precision. But the reduction in noise from averaging to the half-hour (1800 s) can improve effective precision substantially, in the ideal case of pure random white noise, by a factor of sqrt(1800) = 42; in the case of random pink noise, by a factor of $1800^{1/4} = 6.5$; in the case of our development target sensor,

from its 1 s RMS (0.4 ‰) to approximately its Allan variance minimum, $\sigma_{\text{Allan}} = 0.05$ ‰ (table 1).

These results suggest that an optimal design for an eddy covariance sensor will seek to minimize the sensor's Allan variance, not primarily at the short time periods (0.1–1 s) corresponding to high-frequency measurements, but at the required averaging time (typically 20–30 min at forested sites and 10 min over short-stature grasslands or agricultural sites). For eddy flux applications using isotope absorption spectrometry, where achieving sufficient sensor precision is still a technical challenge, this implies that short-term (∼1 s) sensor precision and long-term (∼30 min) sensor stability are co-limiting factors in maximizing the precision of integrated eddy covariance flux measurements.

The real strength of eddy covariance measurements (and the adequacy of the performance of the QCL instrument for such measurements) becomes apparent when measurements accumulated over several days are averaged to produce a tightly constrained mean diurnal curve (simulated for Harvard Forest isofluxes as measured by prototype-quality or development-target quality instruments in figure 7). A dataset of many days or weeks at a time (difficult or impossible to collect with flasks on an ongoing basis) would allow direct observation of how such constrained flux patterns respond to variations in driving variables such as moisture, temperature, and sunlight.

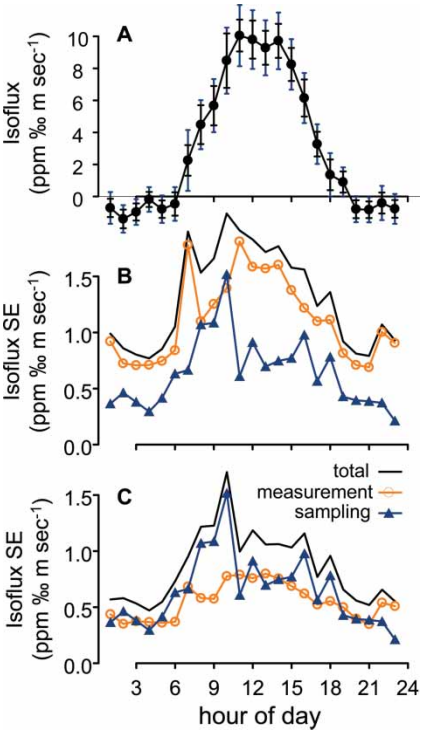

Figure 7. (A) Mean 10-day diel Harvard Forest hourly isoflux covariance ($\overline{w'(\delta^{13}C[CO_2])'} \pm SE_{total}$, $n = 10$ measurement days) simulated from July 2003 eddy data. SE_{total} arises from both sample variation (from day-to-day variations and turbulent noise) and from spectroscopic measurement error, simulated here for both prototype (larger bars) and development target (smaller bars) sensor characteristics. (B) Prototype sensor diel SE_{total} (line) from (A) partitioned into spectroscopic measurement (open circles) and sampling (triangles) error components. (C) Same as (B), but for development of target sensor characteristics. Note that sample variation, which is independent of sensor characteristics, is the same in both (B) and (C).

In both the individual half-hourly time series (figure 6(B)) and in the aggregated 10-day diurnal cycle (figure 7), the portion of the measurement error attributable to instrument noise characteristics is comparable to the inherent meteorological noise associated with turbulent fluxes. This suggests that according to the criterion comparing measurement error to variation associated with turbulent fluxes, the performance of the QCL isotope ratio spectrometer (in particular, the characteristics of the development target instrument) is adequate to measure isofluxes at Harvard Forest as well as they can be expected to be measured.

Although in this article we have focussed on measuring the $^{13}C/^{12}C$ ratios of CO_2 and associated isofluxes, we note that the same laser can be tuned to absorption lines for measuring the oxygen isotopic composition of CO_2 as well, with precision expected to be similar to that obtained for the carbon isotopes. Thus, we expect that a field-deployable version of the prototype discussed here could be used equally well to measure the oxygen isofluxes of CO_2. Indeed, with a dual laser configuration like that outlined in Jiménez *et al.* [33], simultaneous high-accuracy measurement of both carbon and oxygen isotope ratios of CO_2 in the same sample cell should be possible.

The scientific benefit from the capacity to make continuous high-frequency measurements of both δ_{CO_2} and $\delta^{13}C_{CO_2}$ (and associated isofluxes) should be greater than that from making carbon isotope measurements alone, for at least two reasons. Firstly, unlike $^{13}CO_2$ (which because of its typically very tightly constrained relation with CO_2 – figure 4(A) – is straightforward to estimate by combining eddy flux with flask measurements, just as we have done here to simulate carbon isofluxes), there is virtually no other approach for measuring $C^{18}OO$ isoflux above forest ecosystems except for hyperbolic relaxed eddy accumulation, which adds additional technical complexity to the labor-intensive processing of many flask samples [2]. Secondly, the combined information from both isotopes is likely to provide more benefit than the information from just one isotope alone. For example, as recently shown in an analysis by Ogée *et al.* [9], the isotopic disequilibrium between F_{photo} and F_{resp} in equation (1) is almost an order of magnitude larger ($\sim$12–17 ‰) for oxygen than for carbon ($\sim$2 ‰). One of the key limiting factors in using oxygen isotopes for partitioning has been the difficulty in obtaining more accurate $\delta^{18}O_{CO_2}$ isofluxes. Thus, our preliminary experiments with measuring carbon isotope ratios in CO_2 using QCL absorption spectroscopy suggests that this technology shows high potential for oxygen isotopes of CO_2, and hence for making significant scientific progress on the CO_2 flux partitioning problem by multiple approaches.

4. Conclusions

A pulsed-QCL spectrometer operating in the mid-infrared spectral region at 2311 cm^{-1} has sufficient resolution and stability to measure $\delta^{13}C$ of atmospheric CO_2 with the speed and precision needed to enable the calculation of continuous isofluxes by eddy covariance methods. The sensor measurement error in the prototype instrument tested here is comparable to the irreducible 'meteorological' noise inherently associated with turbulent flux measurements above the Harvard Forest ecosystem, but plausible instrument improvements (especially the addition of matched reference cells) can be expected, based on the high performance of an existing $^{12}CO_2$ sensor in which such improvements have already been incorporated, to increase precision to the point where measurement error is less than this meteorological noise. This suggests that QCL-based isotope ratio absorption spectroscopy should approach the precision at which sensor error is not a limiting factor in making eddy covariance measurements of the isotopic composition of CO_2 fluxes.

The key advantages offered by a field-deployable version of this instrument are: (1) the ability to operate continuously without the need for cryogenic cooling (a significant advantage for deployment in remote field sites); (2) increased temperature stability of the isotopologue line-pairs, reducing the need for precise instrumental temperature control; (3) increased signal stability, reducing the frequency of calibration required to maintain high precision to once every 25–30 min. This last advantage would make such an instrument particularly suitable for eddy covariance applications above tall vegetation, where the covariance needs to be integrated for periods of up to 30 min to capture the full spectrum of flux transport.

The performance of this technology in measuring carbon isotope ratios of CO_2 suggests that CO_2 oxygen isotope ratios and associated isofluxes may also be measured. As oxygen isotopes may present additional opportunities for partitioning net ecosystem fluxes of CO_2 into its photosynthetic and respiratory components and a significant limiting factor in oxygen-based CO_2 flux partitioning is the difficulty in accurately measuring isoflux, further development of the QCL-based absorption spectroscopy technology discussed here should present significant opportunities for making progress on the CO_2 flux-partitioning problem.

Acknowledgements

We thank Dave Bowling, David Fitzjarrald, Chun-Ta Lai, Ray Leuning, Frank Tittel, and Steve Wofsy for their valuable advice and discussions. We thank Dan Schrag for isotopic analysis. We thank Antoine Muller, Yargo Bonneti, Guillaume Vanderputte, and Stephan Blaser of AlpesLasers for providing the QCL and the high quality components used in this system, and for their technical advice and assistance. Funding for the instrument development portion of this work has been provided by the US Department of Energy STTR and SBIR programs.

References

[1] D. Yakir, X.F. Wang. Fluxes of CO_2 and water between terrestrial vegetation and the atmosphere estimated from isotope measurements. *Nature*, **380**, 515–517 (1996).

[2] D.R. Bowling, D.D. Baldocci, R.K. Monson. Dynamics of isotopic exchange of carbon dioxide in a Tennessee deciduous forest. *Global Biogeochem. Cy.*, **13**, 903–922 (1999).

[3] H. Craig, L.I. Gordon. Deuterium and oxygen-18 variations in the ocean and the marine atmosphere. *Proceedings of the Conference on Stable Isotopes in Oceanographic Studies and Paleotemperatures*, E. Tongiorgi (Ed.), pp. 9–130, Laboratory of Geology and Nuclear Science, Pisa (1965).

[4] C.J. Barnes, G.B. Allison. Tracing of water movement in the unsaturated zone using stable isotopes of hydrogen and oxygen. *J. Hydrol.*, **100**, 143–176 (1998).

[5] L.B. Flanagan, J.R. Ehleringer. Stable oxygen and hydrogen isotope composition of leaf water in C_3 and C_4 plant-species under field conditions. *Oecologia*, **88**, 394–400 (1991).

[6] G.D. Farquhar, J. Lloyd, J.A. Taylor, L.B. Flanagan, J.P. Syvertsen, K.T. Hubick, S.C. Wong, J.R. Ehleringer. Vegetation effects on the isotope composition of oxygen in the atmospheric CO_2. *Nature* **363**, 439–443 (1993).

[7] P.P. Tans, Oxygen isotopic equilibrium between carbon dioxide and water in soils. *Tellus B* **50**, 163–178 (1998).

[8] L. Stern, W.T. Baisden, R. Amundson. Processes controling the oxygen isotopic ratio of soil CO_2: analytic and numerical modeling. *Geochim. Cosmochim. Acta*, **63**, 799–814 (1999).

[9] J. Ogée, P. Peylin, M. Cuntz, T. Bariac, Y. Brunet, P. Berbigier, P. Richard, P. Ciais. Partitioning net ecosystem carbon exchange into net assimilation and respiration with canopy-scale isotopic measurements: an error propagation analysis with $^{13}CO_2$ and $CO^{18}O$ data. *Global Biogeochem. Cy.*, **18**, GB2019 (2004).

[10] X. Lee, S. Sargent, R. Smith, B.Tanner. *In-situ* measurement of the water vapor O-18/O-16 isotopes ratio for atmospheric and ecological applications. *J. Atms. Ocean. Tech.*, **22**, 555–565 (2005).

[11] J. Ogée, P. Peylin, P. Ciais, T. Bariac, Y. Brunet, P. Berbigier, C. Roche, P. Richard, G. Bardoux, J.-M. Bonnefond. Partitioning net ecosystem exchange into net assimilation and respiration using $^{13}CO_2$ measurements: a cost-effective sampling strategy. *Global Biogeochem. Cy.*, **17**, 1070 (2003).

[12] L.B. Flanagan, J.R. Brooks, G.T. Varney, J.R. Ehleringer. Discrimination against $C^{18}O^{16}O$ during photosynthesis and the oxygen isotopic ratio of respired CO_2 in boreal forest ecosystems. *Global Biogeochem. Cy.*, **11**, 83–98 (1997).

[13] D.R. Bowling, P.P. Tans, R.K. Monson. Partitioning net ecosystem carbon exchange with isotopic fluxes of CO_2. *Glob. Change Biol.*, **7**, 127–145 (2001).

[14] C.-T. Lai, A.J. Schauer, C. Owensby, J.M. Ham, J.R. Ehleringer. Isotopic air sampling in a tallgrass prairie to partition net ecosystem CO_2 exchange. *J. Geophys. Res.*, **108**, 4566 (2003).
[15] C.-T. Lai, J.R. Ehleringer, P. Tans, S.C. Wofsy, S.P. Urbanski, D.Y. Hollinger. Estimating photosynthetic ^{13}C discrimination in terrestrial CO_2 exchange from canopy to regional scales. *Global Biogeochem. Cy.*, **18**, GB1041 (2004).
[16] B. Mortazavi, J.P. Chanton. A rapid and precise technique for measuring $\delta^{13}C$-CO_2 and $\delta^{18}O$-CO_2 ratios at ambient CO_2 concentrations for biological applications and the influence of container type and storage time on the sample isotope ratios. *Rapid Commun. Mass Sp.*, **16**, 1398–1403 (2002).
[17] M.S. Torn, S. Davis, J.A. Bird, M.R. Shaw, M.E. Conrad. Automated analysis of $^{13}C/^{12}C$ ratios in CO_2 and dissolved inorganic carbon for ecological and environmental applications. *Rapid Commun. Mass Sp.*, **17**, 2675–2682 (2003).
[18] M.S. Zahniser, D.D. Nelson, J.B. McManus, P.L. Kebabian. Measurement of trace gas fluxes using tunable diode laser spectroscopy. *Philos. Trans. Roy. Soc. Lond. Ser. A*, **351**, 357–369 (1995).
[19] D. Fowler, K.J. Hargeaves, U. Skiba, R. Milne, M.S. Zahniser, J.B. Moncrieff, I.J. Beverland, M.W. Gallagher. Measurements of CH_4 and N_2O fluxes at the landscape scale using micrometeorological methods. *Philos. Trans. Roy. Soc. Lond. Ser. A*, **351**, 339–356 (1995).
[20] C.V. Horii, M.S. Zahniser, D.D. Nelson, J.B. McManus, S.C. Wofsy. Nitric acid and nitrogen dioxide flux measurements: a new application of tunable diode laser absorption spectroscopy. *SPIE Proc.*, **3758**, 152–161 (1999).
[21] P. Werle, R. Kormann. Fast chemical sensor for eddy-correlation measurements of methane emissions from rice paddy fields. *Appl. Opt.*, **40**, 846–858 (2001).
[22] R. Kormann, H. Müller, P. Werle. Eddy flux measurements of methane over the fen Murnauer Moos using a fast tunable diode laser spectrometer. *Atmos. Environ.*, **35**, 2533–2544 (2001).
[23] J.F. Becker, T.B. Sauke, M. Loewenstein. Stable isotope analysis using tunable diode laser spectroscopy. *Appl. Opt.*, **31**, 1921–1927 (1992).
[24] D.R. Bowling, S.D. Sargent, B.D. Tanner, J.R. Ehleringer. Tunable diode laser absorption spectroscopy for stable isotope studies of ecosystem-atmosphere CO_2 exchange. *Agric. Forest Meteorol.*, **118**, 1–19 (2003).
[25] L. Gianfrani, G. Gagliardi, M. van Burgel, E.R.T. Kerstel. Isotope analysis of water by means of near-infrared dual-wavelength diode laser spectroscopy. *Opt. Express*, **11**, 1566–1576 (2003).
[26] T.J. Griffis, J.M. Baker, S.D. Sargent, B.D. Tanner, J. Zhang. Measuring field-scale isotopic CO_2 fluxes with tunable diode laser absorption spectroscopy and micrometeorological techniques. *Agric. Forest Meteorol.*, **124**, 15–29 (2004).
[27] A. Castrillo, G. Casa, M. van Burgel, D. Tedesco, L. Gianfrani. First field determination of the $^{13}C/^{12}C$ isotope ratio in volcanic CO_2 by diode-laser spectrometry. *Opt. Express*, **12**, 6515–6523 (2004).
[28] C.C. Barford, S.C. Wofsy, M.L. Goulden, J.W. Munger, E.H. Pyle, S.P. Urbanski, L. Hutyra, S.R. Saleska, D. Fitzjarrald, K. Moore. Factors controlling long- and short-term sequestration of atmospheric CO_2 in a mid-latitude forest. *Science*, **294**, 1688–1691 (2001).
[29] S.R. Saleska, S.D. Miller, D.M. Matross, M.L. Goulden, S.C. Wofsy, H. da Rocha, P.B. de Camargo, P.M. Crill, B.C. Daube, C. Freitas, L. Hutyra, M. Keller, V. Kirchhoff, M. Menton, J.W. Munger, E.H. Pyle, A.H. Rice, H. Silva. Carbon in Amazon forests: unexpected seasonal fluxes and disturbance-induced losses. *Science*, **302**, 1554–1557 (2003).
[30] J. Faist, F. Capasso, D.L. Sivco, C. Sirtori, A.L. Hutchinson, A.Y. Cho. Quantum cascade laser. *Science*, **264**, 553–556 (1994).
[31] A.A. Kosterev, R.F. Curl, F.K. Tittel, C. Gmachl, F. Capasso, D.L. Sivco, J.N. Baillargeon, A.L. Hutchinson, A. Cho. Methane concentration and isotopic composition measurements with a mid-infrared quantum-cascade laser. *Opt. Lett.*, **24**, 1764 (1999).
[32] D.D. Nelson, J.B. McManus, S. Urbanski, S. Herndon, M.S. Zahniser. High precision measurements of atmospheric nitrous oxide and methane using thermoelectrically cooled mid-infrared quantum cascade lasers and detectors. *Spectrochim. Acta*, **60**, 3325–3335 (2004).
[33] R. Jiménez, S. Herndon, J.H. Shorter, D.D. Nelson, J.B. McManus, M.S. Zahniser. Atmospheric trace gas measurements using a dual-quantum cascade laser mid-infrared absorption spectrometer. *SPIE Proc.*, **5738**, 318–331 (2005).
[34] M.L. Goulden, J.W. Munger, S.-M. Fan, B.C. Daube, S.C. Wofsy. Measurements of carbon sequestration by long-term eddy covariance: methods and a critical evaluation of accuracy. *Glob. Change Biol.*, **2**, 169–182 (1996).
[35] D.R. Bowling, D.E. Pataki, J.R. Ehleringer. Critical evaluation of micrometeorological methods for measuring ecosystem-atmosphere isotopic exchange of CO_2. *Agric. Forest Meteorol.*, **116**, 159–179 (2003).
[36] J.B. McManus, D.D. Nelson, J.H. Shorter, R. Jiménez, S. Herndon, S. Saleska, M.S. Zahniser. A high precision pulsed QCL spectrometer for measurements of stable isotopes of carbon dioxide. *J. Mod. Opt.*, **52**, 2309–2321 (2005).
[37] J.B. McManus, M.S. Zahniser, D.D. Nelson, L.R. Williams, C.E. Kolb. Infrared laser spectrometer with balanced absorption for measurements of isotopic ratios of carbon gases. *Spectrochim. Acta A*, **58**, 2465–2479 (2002).
[38] D. Weidmann, G. Wysocki, C. Oppenheimer, F.K. Tittel. Development of a compact quantum cascade laser spectrometer for field measurements of CO_2 isotopes. *Appl. Phys. B Lasers O*, **80**, 255–260 (2005).
[39] J.B. McManus, D.D. Nelson, J.H. Shorter, M.S. Zahniser. Quantum cascade lasers for open and closed-path measurement of atmospheric trace gases. *SPIE Proc.*, **4817**, 22–33 (2002).

[40] L.S. Rothman, A. Barbe, D.C. Benner, L.R. Brown, C. Camy-Peyret, K.Chance, M.R. Carleer, C. Clerbaux, V. Dana, V.M. Devi, A. Fayt, R.R. Gamache, J.-M. Flaud, A. Goldman, D. Jacquemart, K.W. Jucks, J.-Y. Mandin, W.J. Lafferty, S.T. Massie, V. Nemtchinov, D.A. Newnham, C.P. Rinsland, A. Perrin, J. Schroeder, K.M. Smith, M.A.H. Smith, K. Tang, J. Vander Auwera, R.A. Toth, P. Varanasi, K. Yoshino. The HITRAN molecular spectroscopic database: edition of 2000 including updates through 2001. *J. Quant. Spectrosc. Radiat. Transfer*, **82**, 5–44 (2003).

[41] D.W. Allan. Statistics of atomic frequency standards. *Proc. IEEE*, **54**, 221–230 (1966).

[42] P. Werle, R. Mucke, F. Slemr. The limits of signal averaging in atmospheric trace-gas monitoring by tunable diode-laser absorption-spectroscopy (TDLAS). *Appl. Opt. B*, **57**, 131–139 (1993).

[43] R. Jiménez, B.C. Daube, J.B. McManus, D.D. Nelson, M.S. Zahniser, S.C. Wofsy. *A new quantum-cascade laser based spectrometer for high-precision airborne* CO_2 *measurements*. Presentation at the 13th WMO/IAEA Meeting of Experts on Carbon Dioxide Concentration and Related Tracer Measurement Techniques, Boulder, Colorado, USA, 19–22 September (2005).

[44] B. Efron, R. Tibshirani. *An Introduction to the Bootstrap*, Chapman and Hall, New York (1993).

[45] K.B. Wilson, D. Baldocchi, E. Falge, M. Aubinet, P. Berbigier, C. Bernhofer, H. Dolman, C. Field, A. Goldstein, A. Granier, D. Hollinger, G. Katul, B.E. Law, T. Meyers, J. Moncrieff, R. Monson, J. Tenhunen, R. Valentini, S. Verma, S.C. Wofsy. Diurnal centroid of ecosystem energy and carbon fluxes at FLUXNET sites. *J. Geophys. Res.*, **108**, 4664 (2003).

[46] J.C. Kaimal, J.J. Finnigan. *Atmospheric Boundary Layer Flows, Their Structure and Measurement*, p. 289, Oxford University Press (1994).